MIXING AND COMBUSTION ENHANCEMENT IN A GENERIC SCRAMJET COMBUSTION CHAMBER

Andreas Mack*, Johan Steelant†
ESTEC ESA, 2200 AG Noordwijk, The Netherlands

and
Klaus Hannemann‡, Sebastian Karl§, Judy Odam**
DLR, Bunsenstrasse 10, 37073 Göttingen, Germany

Abstract

Scramjet engine design (supersonic combustion ramjet) for hypersonic air breathing vehicles is still a challenging topic, since the intake, combustion chamber and nozzle are integrated components of the vehicle. Based on the dimensions of a fullscale vehicle, a generic scramjet combustion chamber was created. The flow conditions for this configuration are taken from typical combustion chambers, Mach 2.5 and 3 with a static pressure of 1 bar and a static temperature of 1300 K. The nonreacting mixing investigations showing significant mixing and penetration improvement by the presence of shocks for this generic combustion chamber have been published earlier. Based on these numerical results of pure mixing, the present work focuses on an improved combustion efficiency due to the shock waves induced by a transversal H_2 fuel injection into the combustion chamber, being reflected at the upper and lower walls of the combustion chamber and interacting with the neighbouring injections. Different injector types (hole, slot, multiple hole inline injector) are investigated and compared concerning combustion efficiency and total pressure loss. The numerical calculations were performed with the unstructured flow solver TAU. As combustion model the Evans/Schexnayder model with 7 species and 8 reactions was used. Near the wall, the combustion process is enhanced depending on the wall temperature. The influence of the combustion on the mixing behaviour is shown. The investigated cases are mainly driven by the mixing behaviour of the gases, the combustion process itself shows only minor contribution to the mixing and combustion enhancement.

I. Introcuction

Scramjet (supersonic combustion ramjet) engines for hypersonic airbreathing vehicles require an adequate design of the propulsion system such that the thrust produced over compensates the drag of the vehicle. The propulsion system itself with inlet, combustion chamber and expansion nozzle have a major contribution to the drag since the vehicle is designed around them. Especially the combustion chamber, due to the total pressure loss and wetted surface area, plays a major rule in the vehicle design. At supersonic combustion, the flow residence time in the combustion chamber is small and the fuel injection, mixing and combustion has to take place inside the combustion chamber. The combustion chamber length is defined by these effects. Achieving fast and homogenous mixing allows to reduce the combustion chamber length and by this also to reduce vehicle drag and structural mass and increase the performance of the vehicle [1]. Combustion efficiencies of 50-95% are targeted.

* Internal Research Fellow, Andreas.Mack@esa.int
† Fluid Dynamics Engineer, Johan.Steelant@esa.int
‡ Head of Spacecraft Section, Klaus.Hannemann@dlr.de
§ Research Engineer, Sebastian.Karl@dlr.de
** Research Engineer, Judith.Odam@dlr.de

In the past, experimental investigations on the interaction and penetration of H_2 injection have been performed and different injector inlet shapes have been considered to increase the mixing [2, 3]. Detailed numerical and experimental work has been done on circular nozzles varying the injection angle [4]. The mixing enhancement of a shock or compression fan induced by a ramp or curved surface was investigated numerically [5], according to this, the mixing efficiency can be improved significantly by the presence of a pressure increase.
Based on this idea, the previous work [6] focused on an improved mixing efficiency due to the shock waves induced by fuel injection in the combustion chamber, being reflected at the upper and lower walls of the combustion chamber and interacting with the neighbouring injections. With this concept, the combustion chamber height and width effects the position of the internal shock system and by this, the mixing behaviour of the injected fuel. Detailed analysis of different combustion chamber cross sections and injector types concerning the mixing efficiencies have been demonstrated [6].

The flow conditions for the generic configuration are taken from typical combustion chambers being 2.5 for the Mach number, 1bar static pressure and 1300K static temperature. The combustion chamber dimensions are related to the fullscale combustion chamber of a future supersonic vehicle. The height of the combustion chamber is fixed at H_{cc}=2H=0.3m. Following the strategy with wall injection on both upper and lower combustion chamber wall, the computational domain employing symmetry conditions is reduced to H=0.15m and a width depending on the injector spacing S=2W. Due to better comparison, the sizes are given dimensionless with the injector diameter being the reference length ($D=L_{ref}$). Ducts with the cross section of WxH=5x5, 5x10, 5x20 and 5x30 are investigated, compare Fig. 1. The injector diameter of D=1 and the width W=5 are kept constant to maintain the ratio of the diameter of the injected fuel jet in relation to the duct width for all cases. The desired equivalence ratio is 1, the fuel injection pressure has to be correlated with the inlet area of the computational domain being dependent on the injector spacing. The combustion chamber length is taken as L/H=12, which corresponds to a dimensional length of 1.8m.
In order to estimate the mixing and combustion performance, the total pressure loss and the mixing or combustion efficiency are calculated. The air based mixing efficiency η_m without combustion at a station of interest x is defined as the ratio of the mass flux of oxygen that would react should the mixture be ignited to the mass flux of oxygen entering the duct:

$$\eta_m(x) = \int_x c_{O_2}^R \, d\dot{m} \,/\, \dot{m}_{O_2,x=0} \tag{1}$$

The mass fraction of the reaction oxygen is:

$$c_{O_2}^R = min\ (c_{O_2}, c_{O_2}^S \cdot c_{H_2} / c_{H_2}^S) \tag{2}$$

The stoichiometric mass fraction of hydrogen $c_{H_2}^S$ corresponds to 0.02876 and the stoichiometric mass fraction of oxygen $c_{O_2}^S$ to 0.22824.
The combustion efficiency η_c at a station of interest x is defined as the ratio of mass flux of reacted hydrogen to the mass flux of hydrogen being injected.

$$\eta_c(x) = 1 - \int_x c_{H_2} \, d\dot{m} \,/\, \dot{m}_{H_2,injected} \tag{3}$$

The total pressure loss due to viscous forces, flow separation, mixing and shock waves is defined as:

$$\Pi(x) = 1 - p_{0,rec}(x) \tag{4}$$

With the pressure recovery being:

$$p_{0,rec}(x) = \frac{\int_x \rho\, u\, p_0 \, dA}{\int_{x=0} \rho\, u\, p_0 \, dA} \tag{5}$$

II. Numerical Modelling

The CFD solutions are achieved with the unstructured DLR TAU-Code that has been validated in the past for different configurations at super- and hypersonic flow conditions [7], including extensive studies for wall jet injection [8]. The time-accurate three-dimensional Navier-Stokes equations are marched for steady or unsteady conditions by an explicit three stage Runge-Kutta scheme or an implicit backward Euler LUSGS scheme. Different standard 2^{nd} order upwind solver such as Van-Leer, AUSM and AUSMDV and gas modelling formulations for perfect gas, thermo-chemical equilibrium and nonequilibrium are available. State of the art acceleration techniques such as local time stepping, residual smoothing and multigrid are implemented as well as turbulence models such as Spalart-Allmaras, k-ω and SST.

The mixing calculations have been performed using a nonreacting mixture model for two perfect gases. Hydrogen and air are modelled as perfect gases employing an additional equation for the 2nd species. The diffusion is modelled by Fick's law with a Schmidt-number of 0.7. The Evans/Schexnayder 7-species 8-reaction set [9] is taken as combustion modeling, the forward reaction rates are describes by an Arrhenius law, whereas the backward rates are calculated by the equilibrium constant

Most computations are performed with laminar wall boundary conditions in order to separate the large scale mixing and diffusion from the influence of the turbulence. Since most full scale models foresee boundary layer bleeds at the combustion chamber entrance, this assumption is reasonable. The generic duct in front of the injector is short so that even turbulent calculations do not have a major effect on the global mixing due to the small boundary layer thickness. Employing thick boundary layers in the range of 2-3 injector diameters at penetrations of 5-6 diameters improves the mixing strongly [10] but are not considered here. Nevertheless, turbulent results are shown to verify this. The hybrid grids are generated with 32 prism cells in the boundary layer and have been locally adapted several times such that the overall number of points is between 10^6 and $1.5 \cdot 10^6$.

III. Results

Mixing results

In the following, some basic results of pure mixing in the generic duct on which the present investigations are based, are shown here. The mixing efficiencies and total pressure losses for different cross sections of the combustion chamber are included in Fig. 2. As can be seen clearly, the mixing efficiency is increased with a higher duct aspect ratio. The 5x5 duct has a better mixing efficiency up to x/H=5 due to an unsteadiness in the flowfield which leads to an improved mixing. This is due to high penetration and a relatively large separation in front of the injector. Although the 5x30 duct has the best mixing capabilities, the mixing gradient for the 5x20 duct is the highest at the end of the combustion chamber. With an increased combustion chamber length, the 5x20 duct would have the best mixing behaviour. Two effects counteract for the different duct cross section sizes. With higher aspect ratio, the absolut hydrogen massflow of each injector is reduced, which leads to a faster mixing. The reduced penetration depth, which is proportional to the square root of the hydrogen massflow, is compensated by the presence of the bowshock, being reflected at the spanwise symmetry planes, for detailed analysis of this phenomenon see [6]. Increasing the cross section aspect ratio diminishes the formation of the rotating vortex in the flowfield, which reduces the mixing capabilities. The 5x30 fails to create a nice vortex, therefore the gradient of the mixing efficiency at the combustion chamber exit is lower than of the 5x20.

The flow topology of the 5x20 duct shows clearly, that the shock pattern of the bow shock due to the interaction with the wall and the symmetry planes increases the penetration further (Fig. 3). The shocks impinging on the hydrogen flow increase the mixing process which can be seen at the hydrogen concentration pattern. The differences in total pressure loss are not significant, they reach approximately 25% at the combustion chamber exit. Due to the

good mixing capabilities, the 5x20 cross section area is taken in the following as a reference model for the combustion investigations.

The mixing performance of different injector shapes and injection Mach numbers for the 5x20 duct are contained in Fig. 4. The supersonic injection takes place at an angle of 60°, otherwise the penetration would be too high. Due to the inclination, the total pressure loss can be reduced by approximately 1-4%, the sonic porthole injection shows the highest total pressure loss. The sonic circular porthole injection shows slightly better mixing performance than the Mach 3 injection. Changing the injector shape to a streamwise slot with the same exit area, but half the spanwise extension increases the mixing efficiency by 8% and reaches 48%, which is almost the performance of the Ma 1 porthole injection. The slanted slot produces a weaker vertical flow, therefore the mixing efficiency reaches only 43%. The injector with 12 inline portholes shows close to the injector the highest mixing efficiency, but later on the fuel is redirected and concentrated at the top symmetry plane in a weak vertical flow which stalls the mixing process at 36%.

Combustion results

In order to study the effects of the combustion modelling on the mixing and combustion behaviour of the injected hydrogen with the incoming air, exactly the same configurations were calculated including the numerical combustion model. The 5x5 duct showed already for the pure mixing case a slightly unsteady behaviour. Including the combustion modelling leads to a strong heat release in the duct, in interaction with the impinging shocks the pressure increase is too large to establish a non-separated flow. Because of this, the equivalence ratio had to be reduced to 0.5 in order to achieve a stable flowfield. The strong vertical flow created by the injector can be seen in Fig. 5. Near the injection plane, a strong formation of water can be observed, whereas in spanwise direction the concentrations reach zero due to the uncombusted air there. In the combustion zone, temperatures reach 3000K (Fig. 6), no ignition delay is observed. The reaction zone begins immediately at the bow shock. The combustion efficiency reaches 30% at the duct exit, which is slightly higher, but comparable with the pure mixing results at Φ=1. The flow further down the duct seems to be mainly mixing controlled, the vertical flow leading to mixing of hydrogen and oxygen, which is ignited immediately due to the high temperature area at the bowshock.

All calculations have been performed for laminar flow so far, nevertheless the impact of the presence of turbulent flow phenomena has to be addressed. Different turbulence models have been applied to this testcase (Spalart-Allmaras, Menter-SST and k-ω), none of them leads to a significant difference in mixing behaviour (Fig. 7). The reason is that the boundary layer is quite thin in relation to the injector diameter and the duct height. On the one hand, the boundary layer begins to grow shortly upstream the injector, which is reasonable for real applications which include a boundary layer bleed in front of the engine combustion chamber. Therefore, the boundary layer does not affect the mixing in the wall near region significantly, especially the separation zone in front of the injector. On the other hand, the penetration for the present cases is so high, that the main mixing and combustion effects take place far away from the walls, where turbulence is only generated by e.g. shear layers and therefore is not dominating the mixing process.
The presence of turbulent flow leads to an increase in total pressure loss of 1-3%. Due to these results, all following cases will be calculated for laminar flow conditions. For other configurations, such as e.g. the HYSHOT configuration; turbulence effects have to be taken into account, if either the boundary layer thickness is large compared to the duct height or the equivalence ratio is low so that the injected fuel stays in the turbulent wall near regions [11].
The 5x20 duct could also not be run at the equivalence ratio of 1 including the combustion process, comparison of the results is therefore not shown here.

Based on analytical relations, it can be shown that the full heat release of a hydrogen combustion at an equivalence ratio of 1 can only be achieved at a Mach number of the main air flow higher than 2.5 for the chosen flow conditions. The Korkegi correlation [12] describes the pressure ratio at which separation of the boundary layer occurs:

$$p_s / p = 1 + 0.3 \cdot (U/a)^2 \quad \text{for} \quad (U/a) < 4.5 \tag{6}$$

For the square of the Mach number much greater that one, the pressure increase due to heat release is [13]:

$$p_c / p = 1 + (\gamma - 1)\Delta Q / a^2 \qquad (7)$$

With T=1300K, ΔQ=3.5MJ/kg, γ=1.3 this leads to a pressure ratio of 3.2, which corresponds according to equation 6 to a required flow Mach number of 2.7. This correlation does not take pressure increases due to shock impingement induced by the injection into account, which lead to local pressure peaks. Due to this, a Mach number of 3 is chosen for the further investigations.

The influence of a variation of the injector diameter (reference diameter of R_j=0.5 and 0.35) for the Mach 3 air flow shows no significant influence (Fig. 8). The local difference in combustion efficiency between x/H=6 and 8 is due to a local subsonic pocket in the injector symmetry plane of the flow domain away from the wall, which is trapped between the bow shock reflections. This region acts as a flameholder and shows large sensitivity on the heat release and pressure increase. Due to that, even with Mach 3 air flow, this configuration is close to choking.
The wall normal sonic hole injection for the 5x20 duct at an air flow Mach number of 3 (R_j=0.5) is compared with the pure mixing results at Mach 2.5. The results show, that the mixing process is not strongly influenced by the combustion process at the duct exit, combustion efficiency is only slightly higher than the mixing efficiency in the vicinity of the injector, further downstream the combustion process once again seems to be driven mainly by the mixing. A potential turbulence combustion coupling should be investigated in the future to confirm this.
Further on, the mixing results of the supersonic slot injection at an inclination of 60° are compared with the combustion calculations of this injector type (Fig. 8). In the previous paper, this configuration was mainly investigated to increase the fuel penetration. Only above x/H=8 the combustion reactions seem to increase the combustion efficiency. This shows, that the combustion process is mainly driven by the mixing behaviour of the gases; the improvement due to the higher local pressure with combustion are rather small for these cases.

For the system level, in order to increase the thrust of the vehicle, it is of advantage to inject with supersonic speed and tilt the injector to align the impulse vector of the injectors with the vehicle x-axis. Systematic variations of injection Mach number and angle were investigated; the results are also shown in Fig. 9.
Concerning the mixing efficiencies, tilting the Mach 1 hole injection improves the combustion behaviour slightly and the total pressure loss is reduced. The slot at Mach 3 at 60° has a better combustion behaviour as the hole, whereas it is significantly reduced if the injection angle is 30°.
Increasing the injection Mach number to 4 (Fig. 9) improves the combustion efficiency once again, at 60° the highest combustion efficiency is reached (55%), but also the largest total pressure loss (66%).
Tilting the injector (Fig. 9) results in reduction of the total pressure losses in the injector vicinity of more than 12%, this effect is reduced until the end of the duct to approximately 8%. The injection Mach number has a minor effect on the total pressure losses, the Mach 3 injectors performs best.
The total pressure losses are in principle linked to the combustion efficiency; higher combustion efficiencies have higher pressure losses. Increasing the Mach number leads for the slot configurations to better combustion efficiency. The Mach 4 slot injectors (30°) have almost the same performance as the Mach 1 hole injectors.

An interesting result is that the gradients of the combustion efficiency at the exit of the duct are identical and roughly linear for all cases (Fig. 8, 9). By this, a required overall duct length can be extrapolated from these results. The length to obtain 100% combustion efficiency vary between 29 and 34 L/H corresponding to 4.35 (Ma 4 injection, 60°) and 5.1m (Ma 3 injection, 30°) for the full scale model (combustion chamber height 0.3m with wall injection from top and bottom wall). A combustion efficiency of 80% would be reached after 22 and 27 L/H (3.3 to 4.1m) for the mentioned cases.

The different combustion efficiencies can be explained by the flow topologies shown here as example for the slot configuration (supersonic injection at Mach 3) at 60° injection angle in Fig. 10 and at 30° in Fig. 11. Due to the weaker bowshock, at a lower angle, which is reflected later at the top symmetry plane and the sidewalls, the interacting with the injected hydrogen occurs for the 30° case at at larger x-values than with the 60° case. The penetration is lower, but still a rotating vortex is formed. Until the duct exit, 8 top-bottom reflections of the bowshock are counted (60°), wheras only 6 take place at 30°. Due to this, the mixing enhancement cannot take full advantage of multiple pressure impingements, although a rotating vortex is formed.

Further on, the influence of the chemical reaction rate model, the wall temperature and the temperature of the main air flow was investigated (Fig. 12). The original reaction set of the Evans/Schexnayder model does not accurately predict the ignition delay due to the exclusion of the hydrogen peroxide H_2O_2 from the reaction set. In order to enforce the combustion process, according to Graddock [14] the formation of OH was enhanced by modifying the Arrhenius coeffients of the correlating reaction equation:

$$O2 + H \rightleftharpoons OH + O \tag{10}$$

For the Arrhenius equation in [cm^3/(mol s)]:

$$K_i = A_i \, T^{B_i} \, e^{-C_i / T} \tag{9}$$

The coefficients of the forward rate constants are $A=2.2 \cdot 10^{14}$, B=0.0 and C=8455 according to Evans/Schexnayder [9]. The forward reactions were enforced by increasing the coefficient A by a factor of three to $6.6 \cdot 10^{14}$.
As can be seen from fig. 12 this modification in the reaction scheme did not enhance the combustion in the flow. Since due to the porthole injection with the detached bow shock and the locally high temperatures there is no ignition delay; further downstream the modified reaction rate also does not have an impact, the timescales of the combustion reactions are much smaller than that one of the flow field which means that the mixing of the flow mainly determines the combustion process.

Increasing the wall surface temperature from 300 to 1000K (Fig. 12) results in slightly higher combustion efficiency (2.5%). It turns out that the portion of fuel, which is inside the separation in front of the injectors bow shock and therefore stays at the wall, burns more rapidly at higher wall temperatures which are in the region of self ignition. Therefore, the combustion efficiencies with 1000K wall temperature are above the ones with 300K right from the injection position.
In addition, the variation of the air flow temperature from 1300K to 1000K is addressed. Since the massflow of air is increasing lowering the temperature, the hydrogen massflow has to be increased to keep the equivalence ratio constant. With an equivalence ratio of 1, the flow separates and the flow chokes. At an equivalence ratio of 0.8 a stable solution could be achieved. As can be seen from Fig. 12, the combustion efficiency doesn't change much until x/H=6, from there a subsonic pocket is established in the middle of the duct close to the injector symmetry plane which enforces the combustion process. The total pressure loss is higher due to the increased absolute injected fuel mass flow.

Finally, some injector modifications are investigated concerning the combustion behaviour. Although penetration and mixing efficiency for the 12-inline injector showed quite good performance in the injector vicinity, the mixing capability, further downstream the duct, vanished since the hydrogen was redirected and concentrated on the top symmetry plane. As for all combustion cases, the air flow Mach number was increased to 3 which changes the flow pattern and results in a smaller bow shock angle. By this, penetration is reduced and the injected fuel does not reach the upper symmetry plane. The flow pattern with the amount of H_2 being left (Fig. 13) and the amount of H_2O being produced (Fig. 14) show the spreading of the fuel and the interaction with the bow shock and its reflections. No strong vertical flow can be observed. Despite this, the combustion efficiency reached is higher than of the reference slot injector, but with increasing x/H the gradient drops slightly such that the maximum combustion efficiency is slightly lower than with the slot injector reference case (Fig. 15). The total pressure loss is also slightly lower (4%). Reducing the injector spacing of the 12 portholes to half the size reduces the combustion efficiency (2%) without reducing the total pressure loss.
For completeness, the 20^o slanted slot injector is included in Fig. 15. For all other injectors, the combustion process slightly increased the mixing process which resulted in higher combustion efficiencies than the corresponding mixing efficiencies. With the slanted slot, the combustion efficiency is reduced by 3% compared with the mixing efficiency of 43% (compare also Fig. 4). Further optimization is needed for this injector type, which shows strong vortical flow in the duct but too low penetration.

The static pressure increase due to the combustion process and the local pressure change due to the bow shock reflections is shown in Fig. 16. Data are plotted at the duct 50% spanwise position along the wall. The static pressure of the air at the inflow is 1 bar. The 5x20 duct with sonic porthole injection shows an averaged monotonous steady increase up to 2.5bar. The impact of the reflected bow shock, which is dominated by the top symmetry plane-wall

reflections can be seen. Injector variations to slot or 12-inline injector show only minor differences in the pressure level, whereas the bowshock reflections impinge at different locations and have different peak values. With the 12-inline injector, the shock reflection impinging on the wall are very strong, since penetration is high, resulting in a relatively large bow shock angle, and the fuel is rather spread than forming a compact jet. Therefore, only weak interaction of the reflected bow shock with the fuel takes place, except the deflection, which results in large pressure peaks (compare also Figs. 13 and 14). At the first impingement point, a small separation occurs which is in good agreement with the Korkegi correlation (eq. 6) which predicts separated flow at a static pressure of 3.7bar. As can be seen, the 5x5 duct (Φ=0.5) also reaches this limit locally; for this reason at higher equivalence ratios the duct choked as mentioned before. The 5x20 duct with a static air temperature of 1000K showed (Φ=0.8) a local subsonic pocket away from the wall. The pressure increases there up to more than 5 bar; increasing the equivalence ratio further was leading to choked flow. The static pressure plots might be misleading, therefore the absolute increase of the flow total enthalpy is plotted along its way along the duct (in Fig. 17). Although the static pressure increase of the 5x5 duct in Fig. 16 is comparable with the other cases the total enthalpy is poorly increased due to the low heat release (Φ=0.5). The supersonic injectors show approximately 20% better performance than the sonic hole injector. Although the configuration with the reduced air temperature of 1000K runs at an equivalence ratio of 0.8, it shows the highest increase in total enthalpy right from the injection point. This is due to the fact that the air mass flow is higher and, as a result, also the massflow of the injected fuel, even at the equivalence ratio of 0.8. This leads to a higher heat release during the combustion process.

Summary

The present investigations show, that the injector configuration and the injector spacing, which is related to the combustion chamber cross section sizes, has an major impact on the flow topology, the shock pattern and as a result on the combustion efficiencies. Compared with previous mixing results, the combustion process does not enhance the mixing of the fuel with the air significantly. If a vortical flow can be established in the duct the combustion efficiency is increased compared with the mixing efficiency. The effects of turbulent flow can be neglected for these configurations, as calculations with different turbulence models show. Nevertheless, in the future a possible turbulence-combustion coupling should be investigated using e.g. an assumed pdf approach.
Higher wall temperatures enhance the combustion process. The total pressure losses are strongly linked with the combustion efficiencies, the highest combustion efficiencies also lead to the highest losses in total pressure.
As could be shown, the combustion efficiencies are strongly dependant on the penetration of the fuel and the capability to form a vortical flow in the combustion chamber. Since this vertical flow is the driver to reach full combustion within the shortest possible combustion chamber length, the flow topology is the main issue to be optimized. Further improvement can be achieved by creating vortical flow actively by e.g. wall shape variations in the combustion chamber or the ramp of the scramjet intake.

Acknowledgments

The numerical work was performed within the ‘Long-Term Advanced Propulsion Concepts and Technologies’ project investigating high-speed airbreathing propulsion. LAPCAT, coordinated by ESA-ESTEC, is supported by the EU within the 6th Framework Programme Priority 1.4, Aeronautic and Space, Contract no.: AST4-CT-2005-012282. Further info on LAPCAT can be found on http://www.esa.int/techresources/lapcat.

References

[1] D. Andreadis, A. Drake, J.L. Garrett, C.D. Gettinger and S.S. Hoxie: "Design considerations of ISTAR hydrocarbon fueled combustor operating in air augmented rocket, ramjet and scramjet modes". 11th AIAA/AAF International Conference on Spaceplanes and Hypersonic Systems and Technologies, Orleans, France, September 29, 2002
[2] M.N. Wendt, R.J. Stalker: "Transverse and Parallel injection of hydrogen with supersonic combustion in a shock tunnel", Shock Waves, Vol. 6, No. 1, Springer-Verlag, 1996

[3] R.C. Orth, J.A. Schetz and F.S. Billig: "The interaction and penetration of gaseous jets in supersonic flow". NASA CR-1386, July 1969
[4] S. Aso, K. Yamaguchi, Y. Tani: "A study on supersonic mixing by circular nozzle with various injection angle for air breathing engine", 57th International Astronautical Congress, 2nd-6th October 2006, Valencia, Spain, 2006
[5] B. Parent and J.P. Sislian: "Hypersonic mixing enhancement by compression at a high convective Mach number". AIAA Journal, Vol. 42, No. 4, April 2004
[6] A. Mack, J. Steelant: "Mixing enhancement by shock impingement in a generic scramjet combustion chamber" European Conference on Computational Fluid Dynamics ECCOMAS CFD 2006, September 5-8 2006,Egmond aan Zee, The Netherlands, 2006
[7] A. Mack, V. Hannemann: "Validation of the Unstructured DLR-TAU-Code for Hypersonic Flows", AIAA 2002-3111, June 2002
[8] A. Kovar, E. Schülein: "Comparison of Experimental and Numerical Investigations on the Side Jets in a supersonic Cross Flow". Royal Aeronautical Society, London, Great Britain, September 14-15, 2004
[9]J.S. Evans, C.J. Schexnayder Jr.: "Influence of Chemical Kinetics and Unmixedness on Burning in Supersonic Hydrogen Flames" AIAA Journal, Vol. 18, No. 2, February 1980
[10] C. Rogers: A Study of the Mixing of Hydrogen Injected Normal to a Supersonic Airstream. Nasa Technical Note, March 1971.
[11] J. Steelant, A. Mack, K. Hannemann and A.D. Gardner: "Comparison of Supersonic Combustion Tests with Shock Tunnels, Flight and CFD", 42nd Joint propulsion Conference & Exhibit, July 9-12, Sacramento, California, AIAA 2006-4684, 2006
[12] R.H. Korkegi: "Comparison of shock-induced two- and three-dimensional incipient turbulent separation", AIAA Journal 1975; 13(4):534-5, 1975
[13] R.J. Stalker, A. Paull, D.J. Mee, R.G. Morgan, P.A. Jacobs: "Scramjets and shock tunnels - The Queensland experience", Progress in Aerospace Sciences, Vol. 41, p. 471-513, Elsevier, 2005
[14] C.S. Graddock: "Computational optimisation of scramjet and shock tunnel nozzles", PhD thesis, University of Queensland, Australia, August 1999

Figures

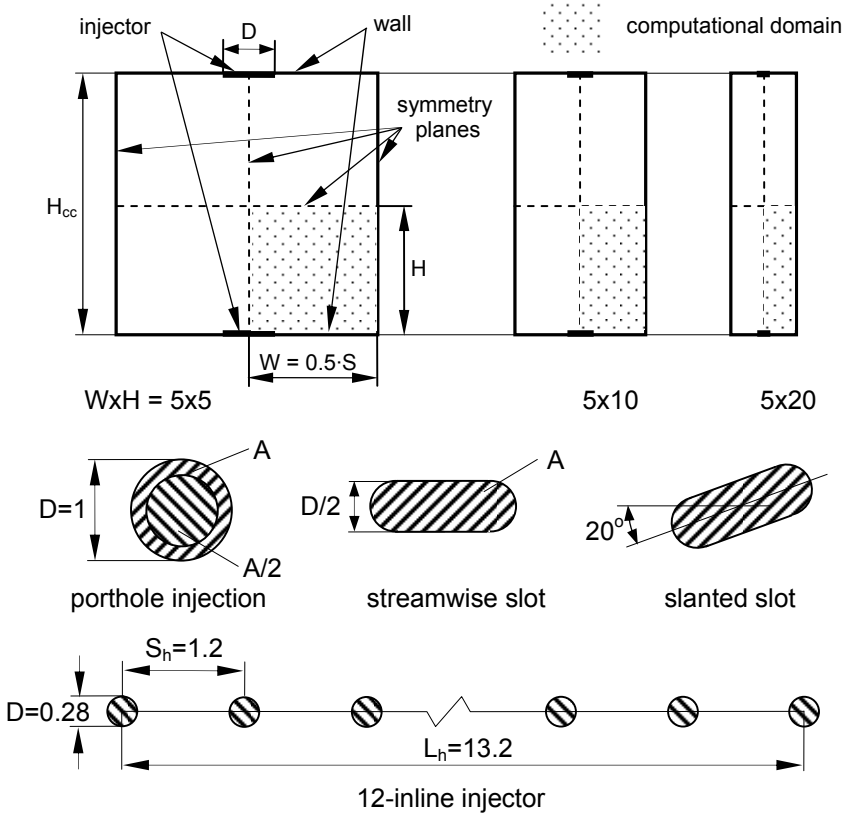

Fig. 1: Geometries: Cross sections of the generic ducts with wall injection from both sides (upper) injector shapes (lower)

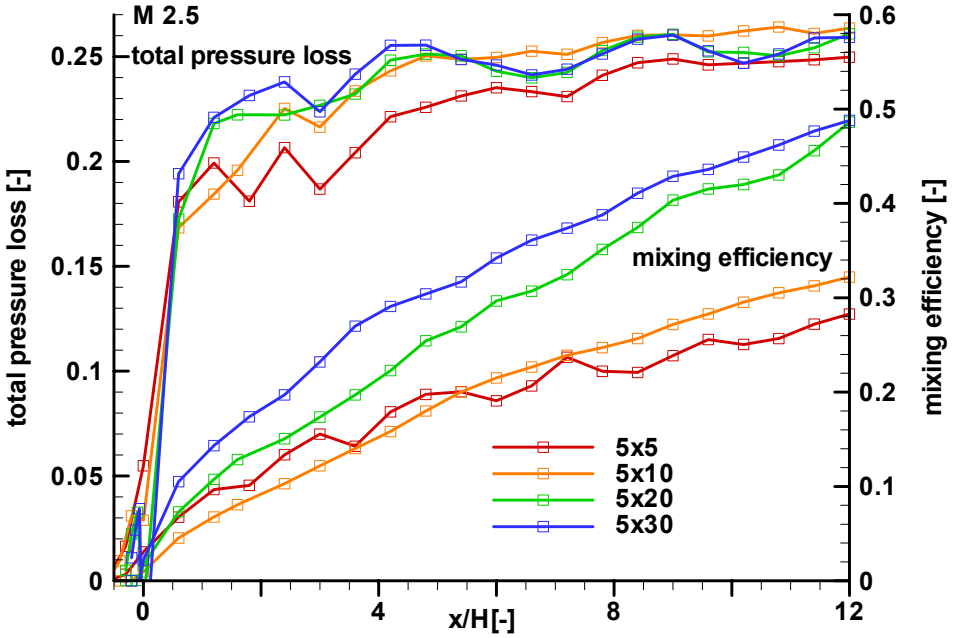

Fig. 2: Mixing efficiency and total pressure loss for 5x5 to 5x30 duct area cross sections

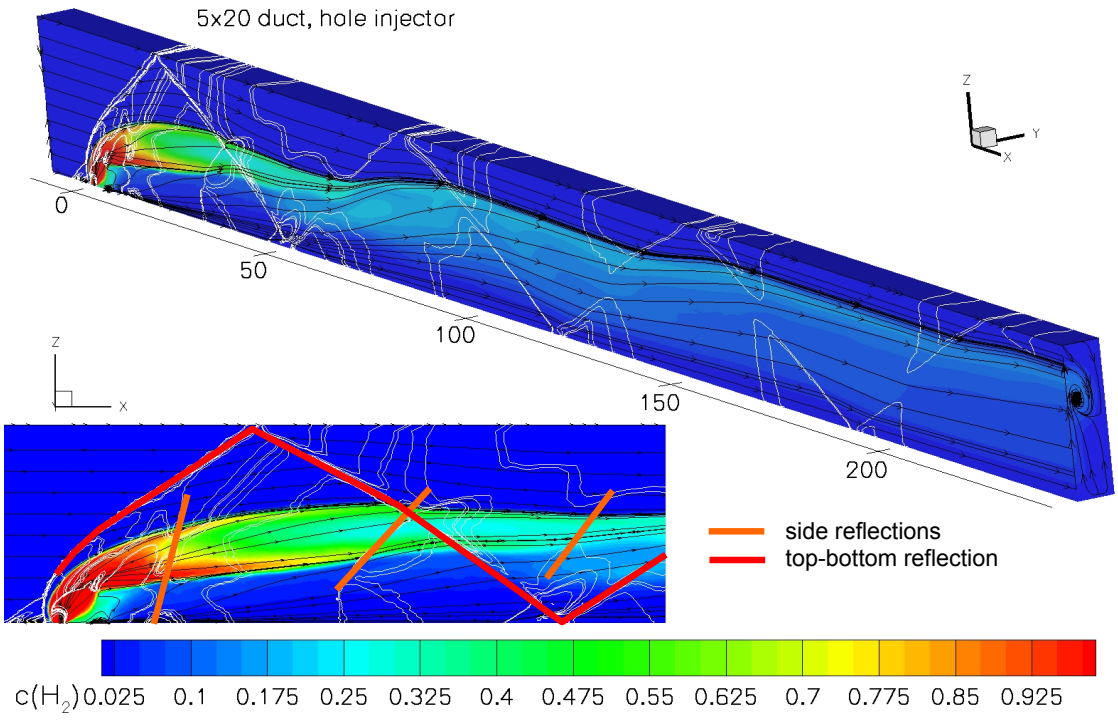

Fig. 3: 5x20 duct, sonic porthole injection: Flowfield topology by streamlines, hydrogen mass fractions and pressure isolines

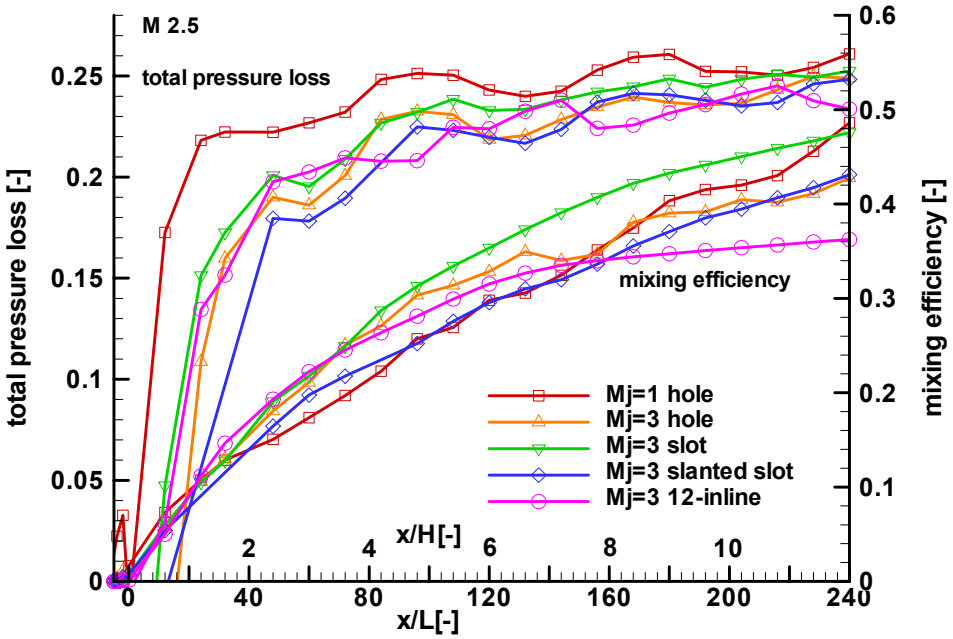

Fig. 4: 5x20 duct: Mixing efficiency and total pressure loss for different injector types

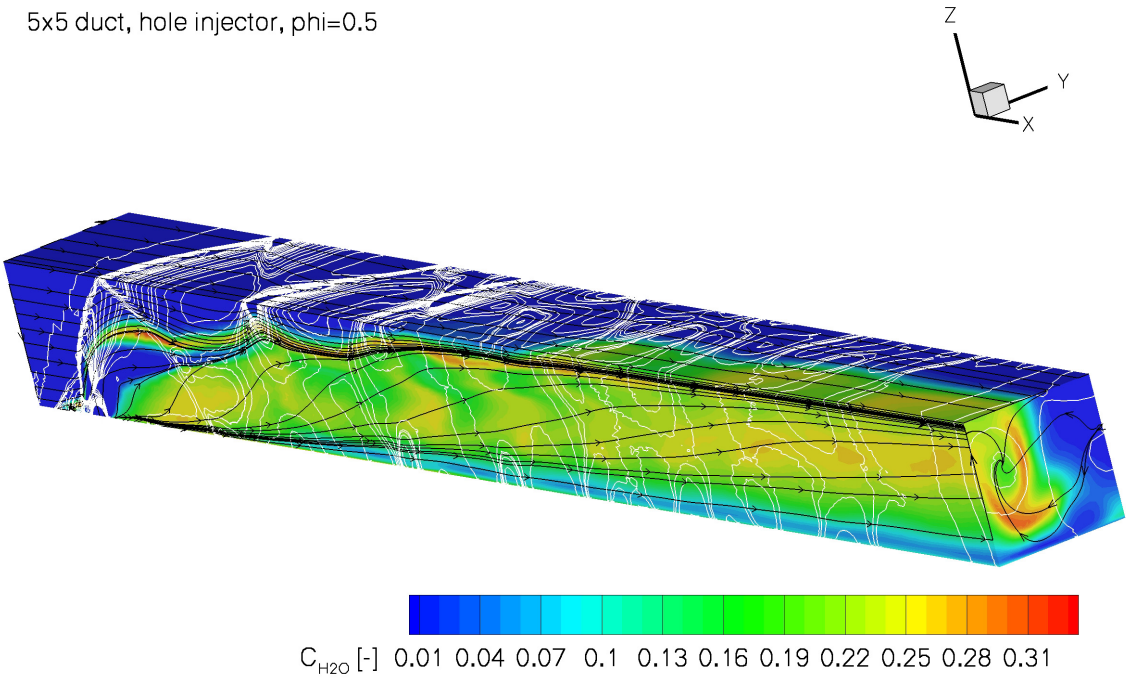

Fig. 5: 5x5 duct with sonic porthole injection (Φ=0.5): Flowfield topology by streamlines, hydrogen mass fractions and pressure isolines

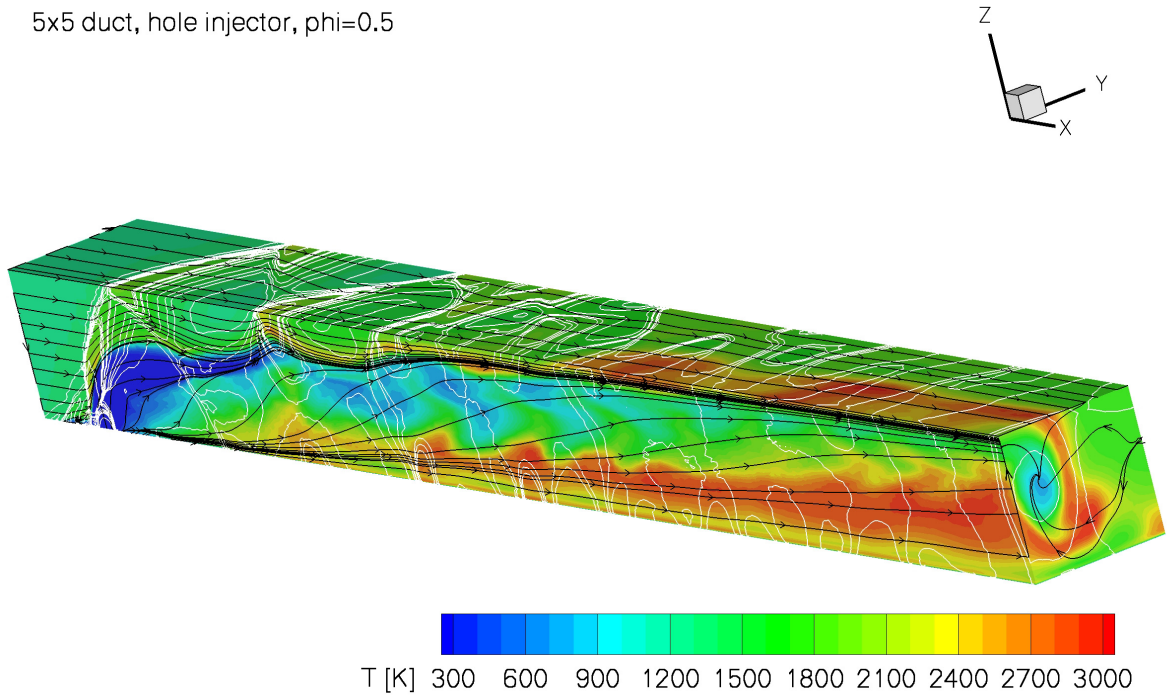

Fig. 6: 5x5 duct with sonic porthole injection (Φ=0.5): Flowfield topology by streamlines, temperature and pressure isolines

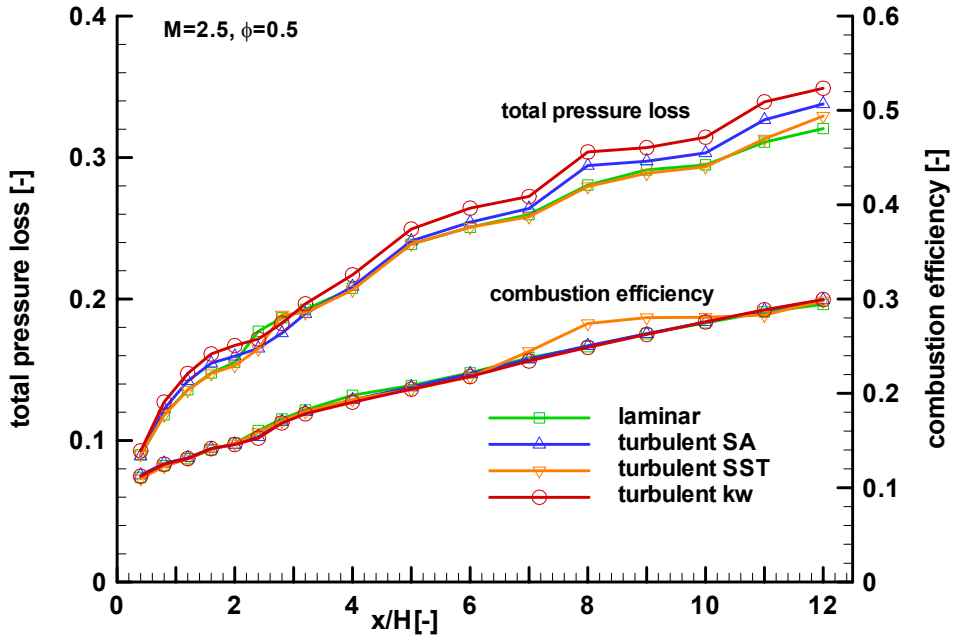

Fig. 7: 5x5 duct (Φ=0.5): Combustion efficiency and total pressure loss for laminar and turbulent calculation

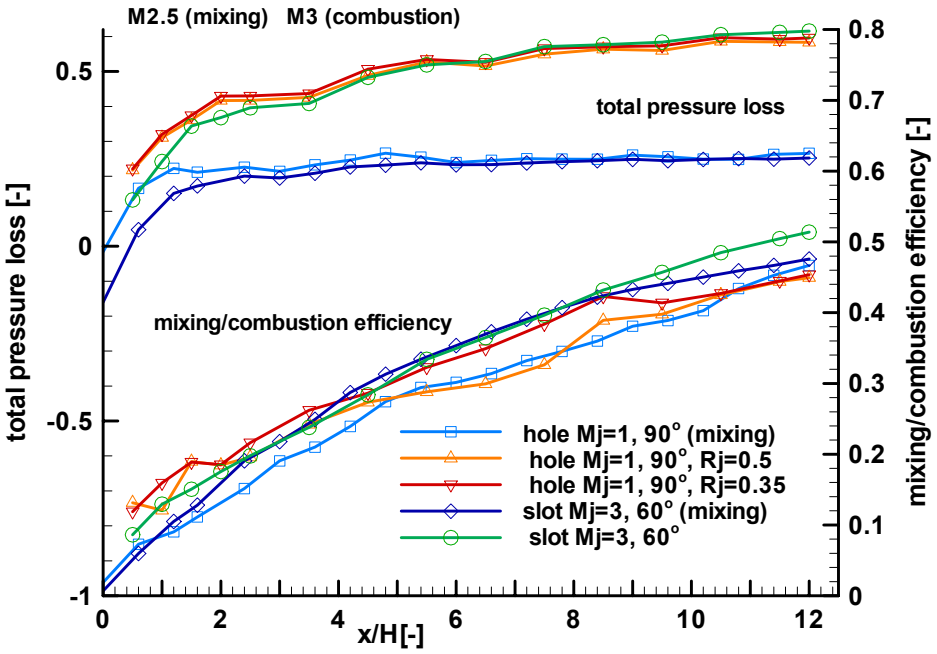

Fig. 8: 5x20 duct: Comparison of mixing (M 2.5) and combustion (M 3) efficiency and total pressure loss for variation of porthole diameter and tilted injection

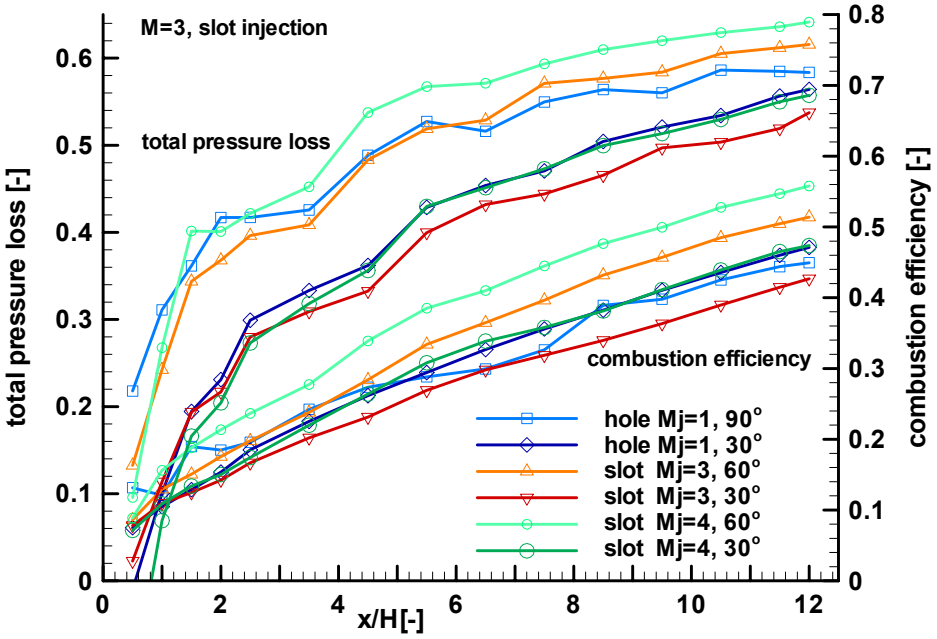

Fig. 9: 5x20 duct: Comparison of combustion efficiency and total pressure loss for porthole and slot injection, variation of injection Mach number and tilting angle

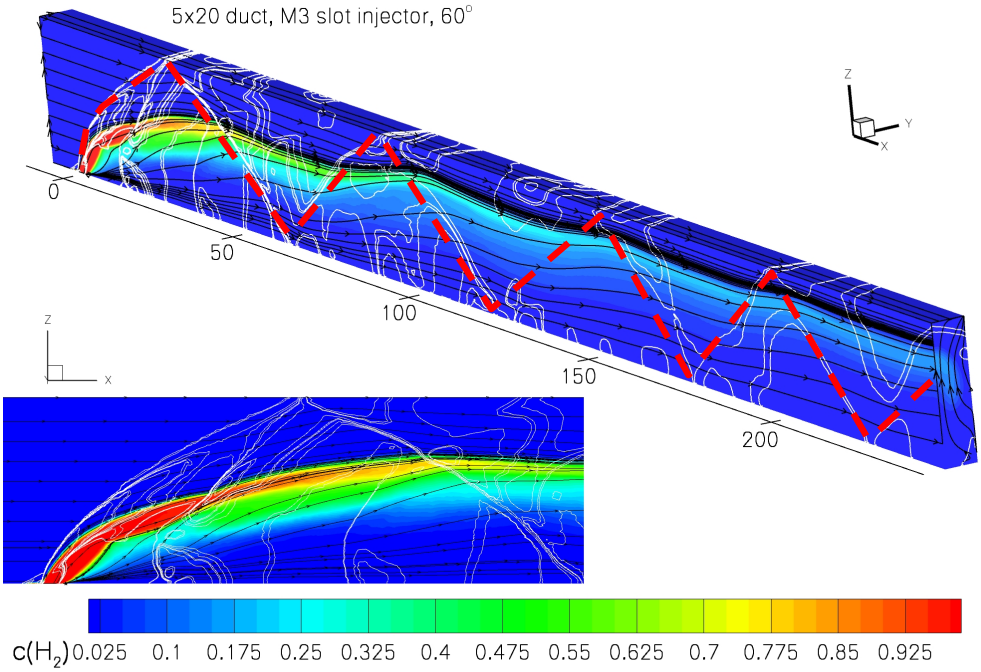

Fig. 10: 5x20 duct, Mach 3 supersonic slot injection at 60°: Flowfield topology by streamlines, hydrogen mass fractions and pressure isolines

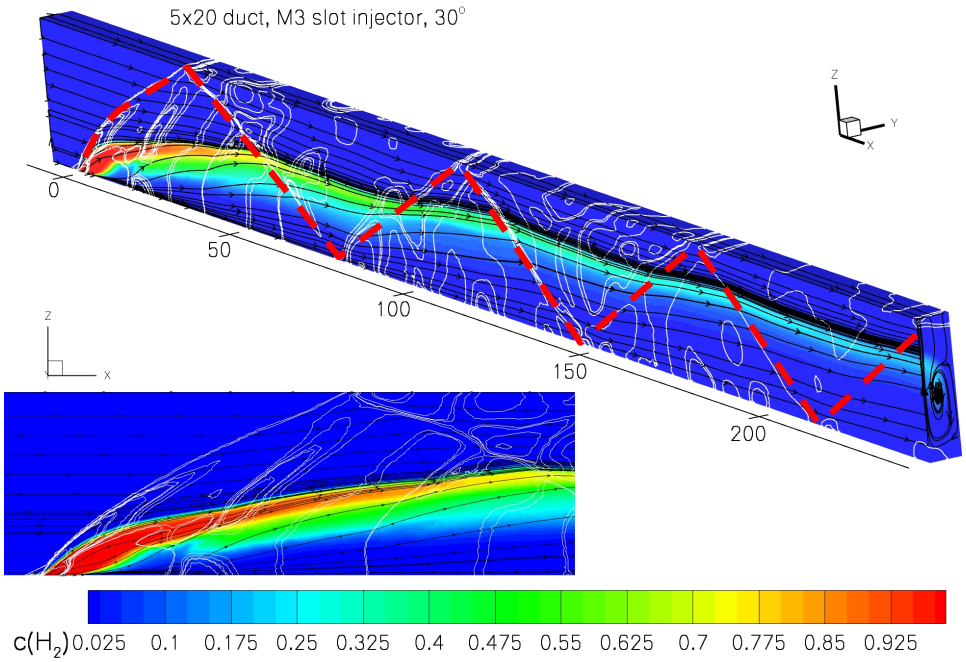

Fig. 11: 5x20 duct, Mach 3 supersonic slot injection at 30°: Flowfield topology by streamlines, hydrogen mass fractions and pressure isolines

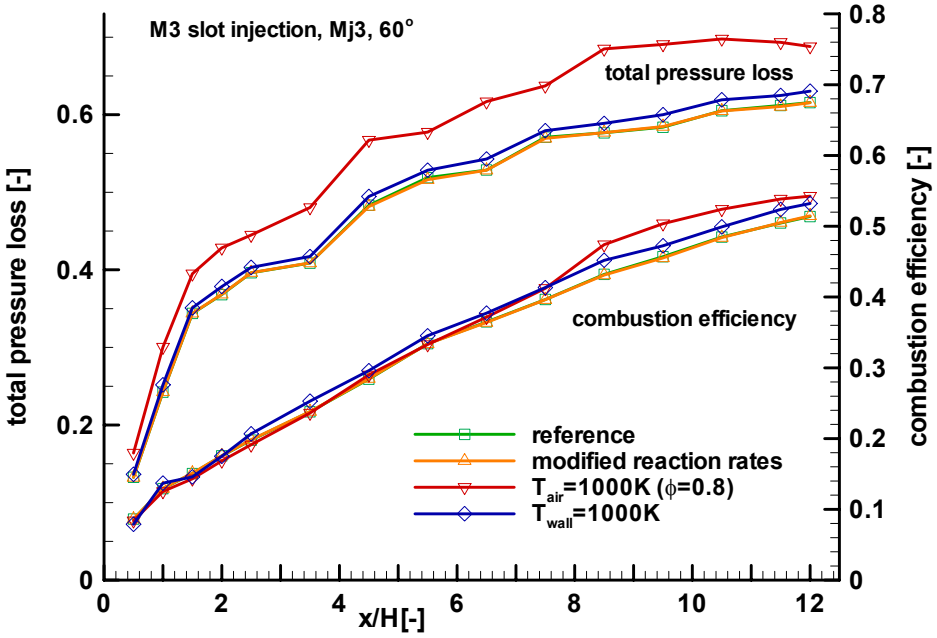

Fig. 12: 5x20 duct, Mach 3 supersonic slot injection at 60°: Comparison of combustion efficiency and total pressure loss for modified combustion reaction rates, air flow temperature and wall temperature

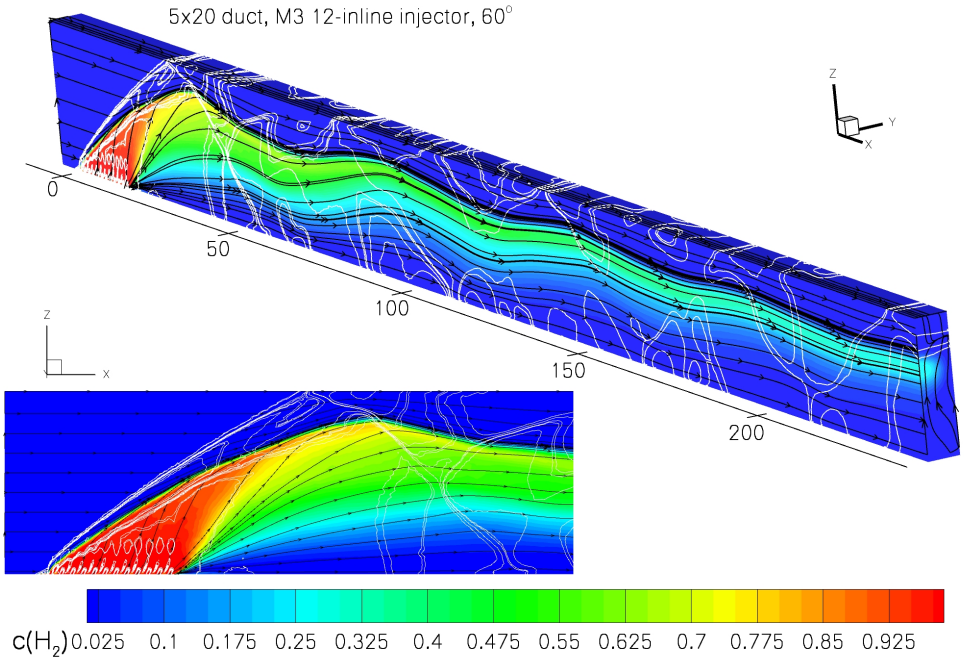

Fig. 13: 5x20 duct, Mach 3 supersonic 12-inline porthole injection at 60°: Flowfield topology by streamlines, hydrogen mass fractions and pressure isolines

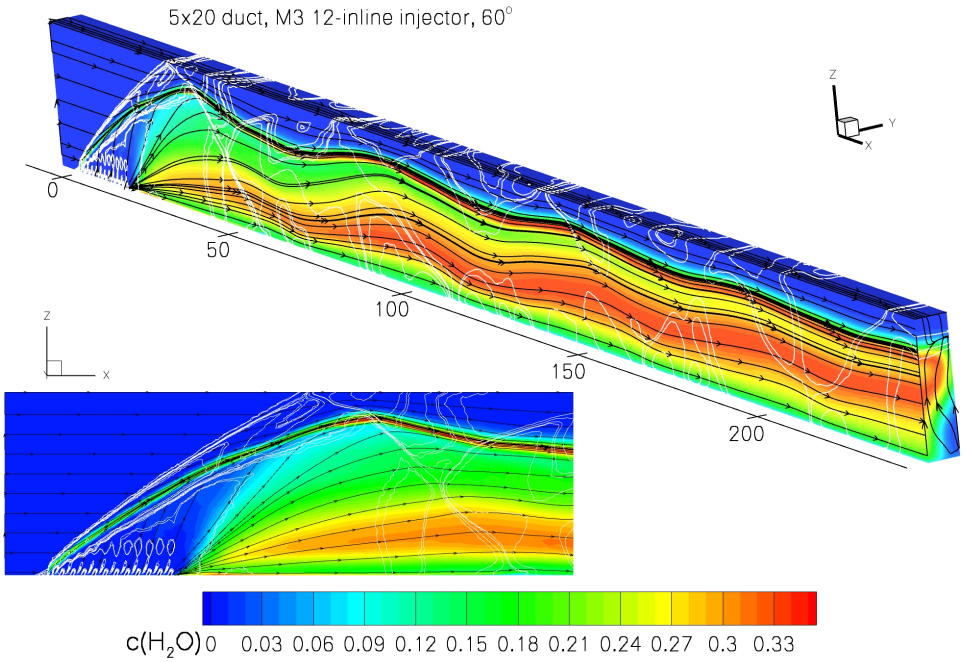

Fig. 14: 5x20 duct, Mach 3 supersonic 12-inline porthole injection at 30°: Flowfield topology by streamlines, H_2O mass fractions and pressure isolines

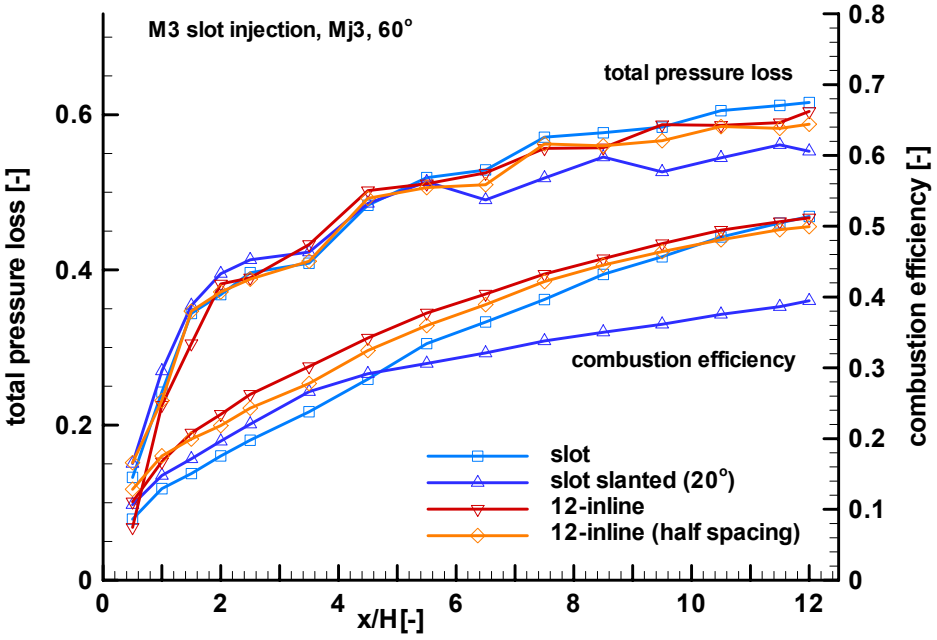

Fig. 15: 5x20 duct, Mach 3 supersonic slot injection at 60°: Comparison of combustion efficiency and total pressure loss for different injector types

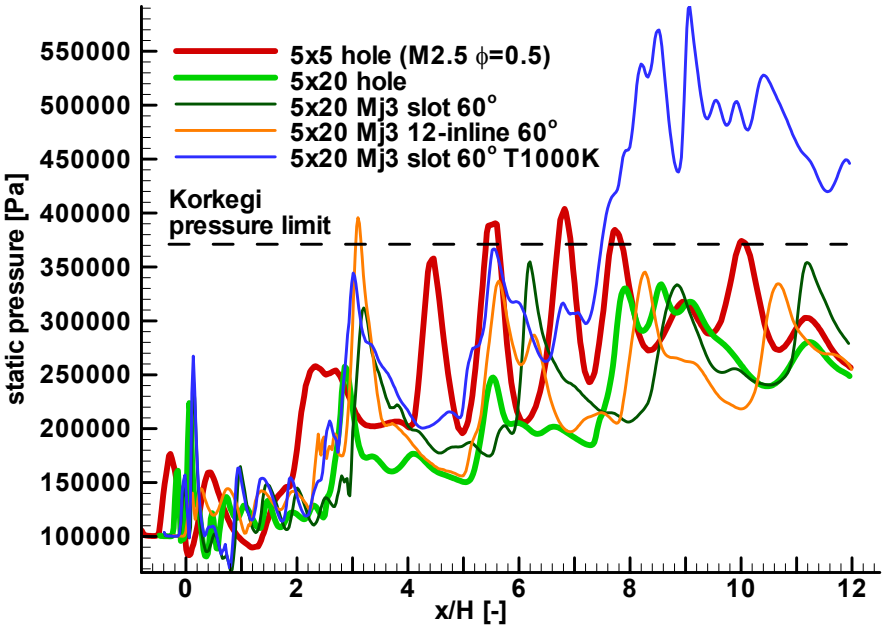

Fig. 16: Static pressure increase at wall spanwise middle section of combustion chamber for different cross sections and injector types

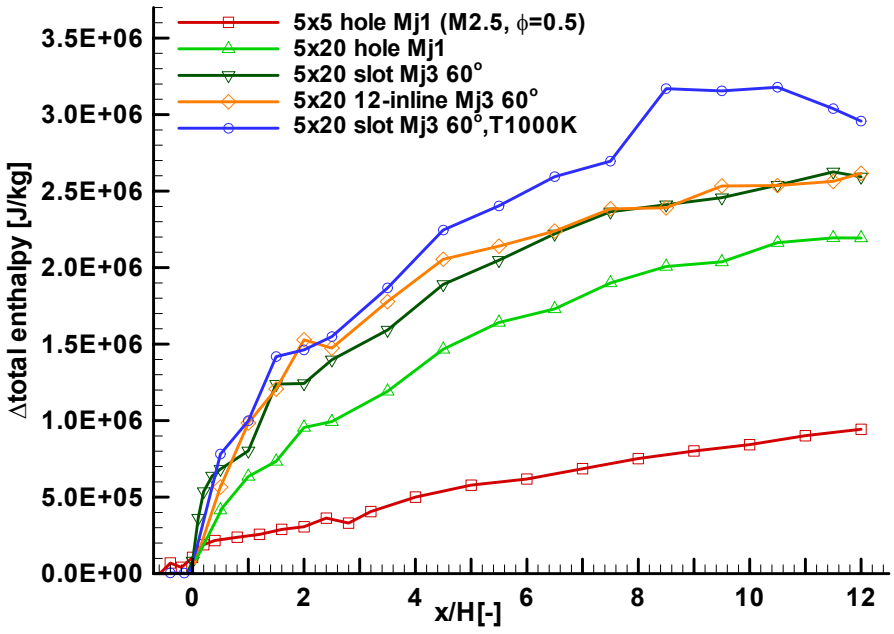

Fig. 17: Total enthalpy increase for different cross sections and injector types